American Society of Hematology
2021 L Street NW, Suite 900,
Washington, DC 20036
Phone: 202-776-0544 | Fax 202-776-0545
editorial@hematology.org

Genome-wide screen identifies Runx2 as a novel regulator of hematopoietic stem cell expansion and T-cell commitment

Tracking no: BLD-2025-029115R1

Grace Meaker (University of Oxford, United Kingdom) Matthew Nicholls (University of Oxford, United Kingdom) Catherine Chahrour (University of Oxford, United Kingdom) Ian Hsu (Weatherall Institute of Molecular Medicine, United Kingdom) Alastair Smith (Weatherall Institute of Molecular Medicine, United Kingdom) Yavor Bozhilov (University of Oxford, United Kingdom) Maurice Ga Hay Leung (University of Oxford, United Kingdom) Hugo Vassort (University of Oxford, United Kingdom) Leonid Olender (University of Oxford, United Kingdom) Oliver Beaven (University of Oxford, United Kingdom) Xinran Huang (University of Oxford, United Kingdom) Elizabeth Brown (University of Oxford, United Kingdom) Marlies Vanden Bempt (University of Oxford, United Kingdom) Hwei Minn Khoo (University of Oxford, United Kingdom) Joydeep Bhadury (Stanford University School of Medicine, United States) Thomas Milne (University of Oxford, United Kingdom) Adam Wilkinson (University of Cambridge, United Kingdom)

Abstract:
Self-renewing multipotent hematopoietic stem cells (HSCs) are a rare but important cell population which can reconstitute the entire blood and immune system following transplantation. Due to their rarity, it has been difficult to comprehensively study the mechanisms regulating HSC activity. However, recent improvements in hematopoietic stem and progenitor cell (HSPC) culture methods using polyvinyl alcohol-based media now facilitate large-scale ex vivo HSC expansion. Here we performed a genome-wide CRISPR knockout (KO) screen in primary mouse HSPCs to discover novel regulators of ex vivo expansion. The screen identified Runx2 as a strong negative regulator of HSC expansion, which we validated using ex vivo and in vivo assays. Loss of Runx2 increased the frequency of immunophenotypic HSCs in HSPC cultures by ~3-fold. Following expansion, these Runx2-KO HSCs engrafted at ~5-fold higher levels in transplantation assays. Non-cultured Runx2-KO HSCs also displayed enhanced reconstitution potential, but loss of Runx2 did not alter blood parameters. Notably however, T-cell reconstitution was diminished from Runx2-KO HSCs, and we further validated an additional role for Runx2 in T-cell commitment using ex vivo and in vivo assays. In summary, we have identified a multifaceted role for Runx2 in HSCs, as a negative regulator of HSC self-renewal and as a facilitator of T-cell commitment. These results will contribute understanding transcriptional regulation of hematopoiesis and improve HSC therapies.

Conflict of interest: COI declared - see note

COI notes: A.C.W. is a consultant for ImmuneBridge. T.A.M. is a paid consultant for and shareholder in Dark Blue Therapeutics Ltd. The remaining authors declare no competing financial interests.

Preprint server: No;

Author contributions and disclosures: G.A.M and A.C.W made the figures and wrote the manuscript. G.A.M., M.N., A.S., Y.B., M.L., H.V., L.O., O.B., X.H., E.B., M.V.B., J.B., and A.C.W., performed the experiments. I.H, H.M.K, C.C, and T.M. assisted with data analysis. A.C.W conceived the study. All authors edited the manuscript.

Non-author contributions and disclosures: No;

Agreement to Share Publication-Related Data and Data Sharing Statement: Sequencing datasets have been deposited on GEO (GSE288012). The datasets will be released following acceptance but are available for review using the token: adgvkawsztspbot

Clinical trial registration information (if any):

Genome-wide screen identifies *Runx2* as a novel regulator of hematopoietic stem cell expansion and T-cell commitment

Authorship

Grace A. Meaker[1], Matthew Nicholls[1], Catherine Chahrour[1], Ian Hsu[1], Alastair Smith[1], Yavor Bozhilov[1,2], Maurice Leung[1], Hugo Vassort[1,2], Leonid Olender[1,2], Oliver Beaven[1], Xinran Huang[1], Elizabeth J. Brown[1], Marlies Vanden Bempt[1], Hwei Minn Khoo[1], Joydeep Bhadury[3], Thomas A. Milne[1], Adam C. Wilkinson[1,2#]

Affiliations

[1]MRC Molecular Haematology Unit, MRC Weatherall Institute of Molecular Medicine, Radcliffe Department of Medicine, University of Oxford, Oxford, UK

[2]Department of Haematology, Cambridge Stem Cell Institute, University of Cambridge, Cambridge, UK

[3]Institute for Stem Cell Biology and Regenerative Medicine, Stanford University School of Medicine, Stanford, USA

[#]Corresponding author. Contact: acw63@cam.ac.uk

Data availability

Sequencing datasets have been deposited on GEO (GSE288012). The datasets will be released following acceptance but are available for review using the token: adgvkawsztspbot

Abstract

Self-renewing multipotent hematopoietic stem cells (HSCs) are a rare but important cell population which can reconstitute the entire blood and immune system following transplantation. Due to their rarity, it has been difficult to comprehensively study the mechanisms regulating HSC activity. However, recent improvements in hematopoietic stem and progenitor cell (HSPC) culture methods using polyvinyl alcohol-based media now facilitate large-scale *ex vivo* HSC expansion. Here we performed a genome-wide CRISPR knockout (KO) screen in primary mouse HSPCs to discover novel regulators of *ex vivo* expansion. The screen identified *Runx2* as a strong negative regulator of HSC expansion, which we validated using *ex vivo* and *in vivo* assays. Loss of *Runx2* increased the frequency of immunophenotypic HSCs in HSPC cultures by ~3-fold. Following expansion, these *Runx2*-KO HSCs engrafted at ~5-fold higher levels in transplantation assays. Non-cultured *Runx2*-KO HSCs also displayed enhanced reconstitution potential, but loss of *Runx2* did not alter blood parameters. Notably however, T-cell reconstitution was diminished from *Runx2*-KO HSCs, and we further validated an additional role for *Runx2* in T-cell commitment using

ex vivo and *in vivo* assays. In summary, we have identified a multifaceted role for *Runx2* in HSCs, as a negative regulator of HSC self-renewal and as a facilitator of T-cell commitment. These results will contribute understanding transcriptional regulation of hematopoiesis and improve HSC therapies.

Key findings

- *Runx2*-deficient HSCs have a fitness advantage *ex vivo* and *in vivo* via increased self-renewal
- *Runx2* is necessary for normal T-cell commitment

Introduction

Life-long hematopoietic system homeostasis relies on a rare population of self-renewing multipotent hematopoietic stem cells (HSCs), which are primarily found within the bone marrow[1,2]. It is estimated that just ~100,000 HSCs sustain the human hematopoietic system[1]. HSCs are also therapeutically important because HSCs will reconstitute the blood and immune system following transplantation into a bone marrow-ablated recipient. This is the basis for stem cell transplantation and related gene therapies. Stem cell transplantation is used clinically to treat a range of blood disorders including leukemias, anemias, and immunodeficiencies[3].

Ex vivo HSC expansion has been proposed as a method to improve HSC therapies. Increasing the numbers of functional HSCs available for therapy could have significant impacts, particularly increasing treatment access and safety. However, stable HSC expansion conditions have long remained challenging. We previously developed a polyvinyl-alcohol (PVA)-based culture system that permits long-term *ex vivo* expansion of transplantable mouse HSCs[4,5]. Within these hematopoietic stem and progenitor cell (HSPC) cultures, transplantable HSCs are found within the $CD201^+CD150^+cKit^+Sca1^+Lineage^-$ ($CD201^+CD150^+KSL$) compartment[6,7], which can be genetically manipulated at high efficiency[8,9]. This polymer-based HSC culture method has recently been adapted for human HSCs[10], highlighting the potential clinical translation of this approach. However, a comprehensive understanding of the molecular regulators of *ex vivo* HSC expansion remains lacking.

The *Runx* transcription factor family consists of *Runx1*, *Runx2*, and *Runx3*[11]. Runx factors contain a conserved Runt protein domain which binds DNA by dimerizing with the common co-binding partner CBFβ[11]. *Runx1* is a well-described hematopoietic transcription factor, required for HSC formation during definitive hematopoiesis[12]. *Runx1* also regulates adult HSPC activity[11] and is commonly mutated in leukaemia[13]. While *Runx3* is less well studied in hematopoiesis, loss has been shown to promote a myeloproliferative phenotype[14] and it has also been shown to prime HSCs for lymphoid differentiation[15]. *Runx2* is primarily thought of as a key regulator of skeletal development[16] and bone cell differentiation[17]. To date, few studies have investigated its role in hematopoiesis. *Runx2* has been reported to display a HSPC-restricted expression pattern, and to regulate myelopoiesis in normal and leukemic contexts[16,18]. In particular, *Runx2* has also been shown to be important for the development of plasmacytoid dendritic cells (pDCs)[19]. Despite this, there are no reported roles for *Runx2* in HSC self-renewal or fitness.

Here, we used a genome-wide CRISPR screen approach to identify *Runx2* as a potent negative regulator of HSC expansion *ex vivo*. Alongside boosting HSC expansion *ex vivo*, we also discovered that expanded *Runx2*-KO HSCs more efficiently reconstitute the myeloid and B cell lineages *in vivo* following transplantation. We have also discovered that *Runx2* is required for the normal development and reconstitution of T-cells.

Materials and Methods

Reagents referenced in this methods section are detailed in **Table S1-2**.

Mouse models

All experiments were initiated with 8-12-week-old mice and were approved by the UK Home Office. This study used two different Cas9-expressing mouse lines purchased from the Jackson Laboratory and bred in house: (1) the doxycycline-inducible Cas9-expressing line, C57BL/6-Gt(ROSA)26Sor$^{tm1(rtTA*M2)Jae}$ Col1a1$^{tm1(tetO-cas9)Sho}$ (JAX:029415); and (2) the constitutive Cas9-expressing line, C57BL/6-Gt(ROSA)26Sor$^{tm1.1(CAG-cas9*,-EGFP)Fezh}$ (JAX: 024858). We also generated *Runx2*-KO mice by crossing *Runx2*$^{tm1.1Tok}$ (MGI:6874594[20]) with B6.Cg-*Commd10*$^{Tg(Vav1-icre)A2Kio}$/J (JAX:008610[21]) for hematopoietic-specific *Runx2* deletion. C57BL/6-CD45.1 and C57BL/6-CD45.1/CD45.2 were bred in house while C57BL/6-CD45.2 were purchased from Envigo.

Ex vivo HSPC cultures

Bone marrow was collected and stained with APC-c-Kit antibody and then with anti-APC magnetic beads, before MACS column enrichment[8]. Bone marrow c-Kit$^+$ HSPCs were plated into 24-well CellBIND plates in PVA-based media[4,8] described in **Table S3** and incubated at 37°C with 5% CO_2 and 5% O_2. Complete media changes were performed every 2-3 days. Cultured HSCs were transferred to fibronectin-coated plates for lentiviral transduction at indicated timepoints and then returned to CellBIND plates for further culture.

Ex vivo HSPC CRISPR screen

Following an initial 17-day *ex vivo* expansion, ~100 million constitutive Cas9-expressing HSPCs (with a CD201$^+$CD150$^+$KSL cell frequency at ~10%; **Figure S1A**) were transduced with the Gouda genome-wide lentiviral sgRNA KO library (Addgene #73633[22]). High titer lentivirus library was generated from HEK 293T cells (in DMEM supplemented with sodium 10 mM pyruvate, 2 mM GlutaMax, 4.5 mM sodium propionate, 2mM sodium butyrate, 1.5 mM caffeine, and 5% heat-inactivated FBS), concentrated by ultracentrifugation, and titrated using K562 cells[23]. HSPCs were transduced for 6 hours at an MOI of 0.3, then recovered for

48 hours before being puromycin selected (1 ug/ml) for 48-hours prior to collection of the t0 timepoint. Droplet digital PCR on genomic DNA collected following puromycin selection confirmed ~0.8 virus integration per genome (**Figure S1B**). This genome-wide HSC KO library was split into two technical replicates and expanded another 21-days, with samples collected at t7, t14, and t21. Following gDNA extraction, sgRNAs were PCR amplified for next generation sequencing. The MAGeCK pipeline[24] was used to analyze the dataset.

Lentiviral gene knockouts

Guide sequences (**Table S4**) were acquired from the Bassik lab CRISPR knockout library[25] or designed using the WGE Sanger tool[26] and cloned into the pMCB306 lentiviral plasmid (Addgene #89360). As controls, a *Rosa26*-targeting sgRNA and a non-targeting sgRNA were used. Lentivirus was then produced by transfection of HEK293T cells and HSPCs were transduced on day 14 of culture. For experiments using dox-inducible Cas9 cells, Cas9 was induced by the addition of 500 ng/ml doxycycline for 48-hours at 48-hours post-transduction. HSPCs were collected at indicated time points for assays detailed below.

Flow cytometry and sorting

HSPC cultures, peripheral blood, bone marrow, thymi, spleens and T-cell differentiations were stained using the relevant antibody cocktails (**Tables S5-17**) and then analyzed on a BD Fortessa or sorted on a BD FACS Fusion. For intracellular flow cytometry, cultured HSPCs were fixed and permeabilized using the BD Pharmigen Transcription Factor Buffer Set and then antibody stained for 40 minutes with anti-RUNX2-PE or an IgG isotype control.

HSC transplantation

For CRISPR *Runx2*-KO experiments, C57BL/6-CD45.1 mice were lethally irradiated (12 Gy) and received tail vein injections of 2000 $CD201^{+}CD150^{+}$KSL cells and 1 million whole bone marrow competitor cells. For *Runx2*-flox KO experiments, lethally irradiated C57BL/6-CD45.1 mice received either 100 fresh bone marrow $CD150^{+}CD34^{-}$KSL HSCs and 1 million whole bone marrow competitor cells, or 10,000 day-14 cultured cells (initiated from $CD150^{+}CD34^{-}$KSL HSCs) and 1 million whole bone marrow competitor cells. Peripheral blood was taken every 4-weeks and analyzed via flow cytometry using the panel in **Table S9**. At the endpoint, bone marrow cells were collected and stained with the panels in **Table S10-11** for flow cytometry. Secondary transplant assays were performed using 5 million whole bone marrow from primary recipients.

CUT&Tag chromatin profiling

CUT&Tag was performed as described previously[27] using anti-RUNX2 and anti-H3K4me3 antibody (**Table S1**). Libraries were 150bp paired-end sequenced with a NovaSeq (Illumina, Novogene). Quality checking of FastQ files was performed using FastQC (v0.12.1)[28]. The reads were trimmed using Trim Galore (v0.6.10)[29]. Bowtie2 (v2.5.1) was then used to map the trimmed reads to the mm39 reference genome[30]. Bigwigs were produced using deeptools bamCoverage (v3.5.1)[31] and visualised using computeMatrix and plotHeatmap (v3.5.1)[31]. Peaks were called using LanceOtron callPeaks[32]. De novo motif discovery was performed using Streme (v5.5.3)[33], and enriched motifs were compared to the HOCOMOCO (v12) database using Tomtom (v5.5.3)[33,34]. Raw motif analysis data can be found in **Table S18.**

Transcriptomic analysis

RNA from FACS-isolated $CD201^+CD150^+$KSL immunophenotypic HSCs (n=3) and $CD201^-CD150^-$KSL hematopoietic progenitor cells (HPC; n=3) were extracted using the Direct-zol RNA Microprep kit. Libraries were 150bp paired-end sequenced with a NovaSeq (Illumina, Novogene). Quality checking of FastQ files was performed using FastQC (v0.12.1)[28]. The reads were trimmed using Trim Galore (v0.6.10)[29]. STAR (v2.7.10b) was then used to map the trimmed reads to the mm39 reference genome[35]. Quantification of gene expression was performed using featureCounts (v2.0.3)[36]. Differential gene analysis was performed using DESeq2 (v1.40.2)[37]. GO over representation analysis was performed using Cluster Profiler (v4.10.1)[38]. Raw datasets can be found in **Tables S20-S22**.

Ex vivo T-cell differentiation

Biotinylated recombinant human DLL4 was incubated with streptavidin-coated polystyrene particles at 30 minutes at room temperature to generate DLL4-µBeads. $1\text{-}20\times10^3$ cells from indicated 14-day HSPC cultures were differentiated with 1×10^5 DLL4-µBeads in the media described in **Table S23**. After 7 days incubation at 37°C in 5% CO_2, cells were harvested for flow cytometry using the panel in **Table S10**.

Results

An ex vivo CRISPR KO screen identifies putative regulators of HSC expansion

To comprehensively identify the regulators of *ex vivo* HSC expansion potential, we performed a genome-wide CRISPR KO screen during a PVA-based mouse HSPC expansion culture (**Figure 1A**). Whilst these cultures are heterogenous, they enable cell culture scales sufficient for a genome-wide screen. Following CRISPR library transduction and puromycin selection, we collected samples weekly for 3-weeks (t0-t21) for sgRNA

sequencing. We detected essentially all sgRNAs throughout the 21-day screen, although the library compositions slowly changed over time (**Figure S1C**). We performed MAGeCK analysis[24] to identify statistically-significant regulators of HSPC expansion in these *ex vivo* conditions.

From this screen analysis, we identified both putative essential genes with a negative effect (beta) score (where sgRNAs abundance decrease over time) and putative negative regulators with a positive effect score (where sgRNA abundance increases over time) (**Figure 1B; Table S24**). Initially focusing on the 2305 statistically-significant essential genes (FDR<10%), we compared them with the Achilles common essential list[39] (containing 1552 genes). While 995 were also found in the Achilles list, 1310 appeared to be HSPC-specific essential genes (**Figure 1C**). Several of these are previously reported regulators of HSPC activity (e.g. *Gata2*[40,41], *Lmo2*[41,42]). However, the list also contains various novel putative essential genes for the growth and/or survival of HSPCs in PVA-based cultures.

Given our interest in identifying mechanisms to boost HSC expansion, we focused on the putative negative regulators of ex vivo expansion. Our screen identified 92 statistically significant (FDR<10%) hits (**Figure 1B**). This again included reported HSC negative regulators (e.g. *Trp53*[43], *Pten*[44]) and novel putative regulators. To better understand the potential biological networks negatively regulating HSPC expansion, we performed STRING analysis[45] (**Figure 1D**). The transcription factor *Runx2* appeared in this analysis as a well-connected node, but one that had not to our knowledge been previously implicated in regulating HSC expansion. We confirmed that *Runx2*-targeting sgRNAs increased ~5-fold during the screen (**Figure 1E**). This was notably higher than the other Runx family members, *Runx1* and *Runx3*, which appeared to be more modest negative regulators of HSPC expansion (~3-fold) and did not reach statistical significance (**Figure 1E**). These results suggested *Runx2* as a novel negative regulator of *ex vivo* HSC expansion.

Loss of Runx2 enhances HSC fitness but inhibits T-cell output

Given that *Runx2* was one of the top putative negative regulators in our HSPC expansion screen, yet played an unknown role in HSC activity, we sought to validate this hit. First, we validated that RUNX2 was expressed in the majority of our cultured HSCs via flow cytometry (**Figures S2A-B)**. RUNX2 expression in *ex vivo* HSCs was similar to freshly-isolated HSCs, but lower than in pDCs, which are known to highly express RUNX2[19] (**Figure S2C**). Next, we performed targeted deletion of *Runx2* in our *ex vivo* HSPC cultures by transducing dox-inducible Cas9-expressing HSCs with lentivirus encoding *Runx2*-targeting sgRNAs or control

sgRNAs (*Rosa26*-targeting sgRNA, non-targeting sgRNA) (**Figures 2A-B**). We confirmed that these sgRNAs induced loss of RUNX2 protein expression (**Figure 2C)**. We then tracked the frequency of immunophenotypic $CD201^+CD150^+$KSL (p)HSCs[6,46] (**Figure 2D-E; Figure S2D**) and KSL (p)HSPCs for 3-weeks following dox-mediated Cas9 induction (**Figure S2E**). Loss of *Runx2* progressively increased the pHSC frequency to ~3-fold by day 21 (**Figure 2E**). These results confirmed our CRISPR screen identification of *Runx2* as a negative regulator of pHSC expansion.

We were next interested in determining the functional consequences of *Runx2* loss. We performed HSC transplantation assays in $CD45.1^+$ lethally irradiated mice. To account for the increased frequency of pHSCs in the *Runx2*-KO cultures, we sorted and transplanted 2000 $CD45.2^+$ pHSCs from 14-day *Runx2*-KO and control HSC cultures per recipient alongside 1 million $CD45.1^+CD45.2^+$ whole bone marrow competitor cells (**Figure 2F**). Donor chimerism was then tracked monthly in the peripheral blood (**Figure S2F**). Given the similar phenotypes between the two control sgRNAs and the two *Runx2*-targeting sgRNAs, the results have been merged for ease of visualization.

Even from the earliest 4-week timepoint, the frequency of *Runx2*-KO HSC-derived cells was higher in the peripheral blood; ~75% compared to ~30% of control cells (**Figure 2G**). This enhanced donor chimerism was sustained in the peripheral blood (myeloid, T- and B-cells) throughout the 20-week time course in the *Runx2*-KO recipients, while donor chimerism in the control cohort gradually dropped to ~15% (**Figure 2G-H**). Endpoint bone marrow analysis also confirmed correspondingly high chimerism; ~90% donor chimerism in the *Runx2*-KO recipients as compared to ~10% in the controls (**Figure 2I; Figure S2F**). Within the bone marrow, we also observed a modest (~2-fold) increase in KSL frequency (**Figure S2G**), in line with the *ex vivo* phenotype.

Within the *Runx2*-KO HSC recipients, blood parameters appeared normal in complete blood count analysis, suggesting that loss of *Runx2* did not block blood production (**Figure S2H**). However, further investigation identified a lineage output bias from the *Runx2*-KO HSCs. Within the *Runx2*-KO HSC-derived peripheral blood cells, B-cell frequency was enhanced while T-cell frequency was correspondingly depleted (**Figure 2J**) compared to control HSCs. The frequency of myeloid cells was unaltered. Secondary transplantation assays confirmed that *Runx2*-KO HSCs sustained high peripheral blood and bone marrow chimerism long-term (**Figure S2I-J**). Together, these results suggest that loss of *Runx2* provides HSCs with a fitness advantage while inhibiting T-cell potential.

Heterozygous loss of Runx2 is sufficient to increase HSC expansion and engraftment

To further investigate the role of *Runx2* in hematopoiesis and to better understand the importance of *Runx2* dosage *in vivo*, we bred and characterized a *Runx2*^{flox} *Vav1-iCre* transgenic mouse line (**Figure 3A**). Analysis of the bone marrow, spleen and thymus from *Runx2*$^{flox/flox}$ *Vav1-iCre*$^{+}$ (*Runx2*-hom KO) and *Runx2*$^{flox/wt}$ *Vav1-iCre*$^{+}$ (*Runx2*-het KO) adult mice (8-12-weeks) revealed no gross changes associated with unperturbed hematopoiesis compared to wild-type (*Runx2*-wt) controls (**Figures S3A-G**). This was in line with our *Runx2*-KO transplant recipients and a previous report that did not observe changes in blood parameters[47].

To understand whether loss of *Runx2* altered HSC activity without *ex vivo* culture, we performed transplantation assays using freshly-isolated *Runx2*-hom, *Runx2*-het KO and *Runx2*-wt HSCs. *Runx2*-hom displayed higher long-term donor peripheral blood and bone marrow chimerism (**Figures 3B-C**). Again, the lineage output of the peripheral blood showed a decreased T-cell output in the *Runx2*-hom KO donor cells. To our surprise, *Runx2*-het KO HSCs largely recapitulated the boost in reconstitution potential, although they did not display reduced T-cell output (**Figure 3D**). No gross changes in hematopoiesis were observed in any of the recipient groups (**Figure S3H**).

We next investigated how *Runx2* dosage influenced HSC expansion. Both *Runx2*-hom KO and *Runx2*-het KO HSCs displayed a similar phenotype to our CRISPR KOs *ex vivo*, generating higher pHSC frequencies (**Figure 3E**). *Runx2*-hom and *Runx2*-het KO HSC cultures also engrafted at similar levels in transplantation assays, and significantly higher than *Runx2*-wt controls (**Figures 3F-H**). Again, the complete blood cell counts showed no gross changes in hematopoiesis (**Figure S3I**). Finally, we performed secondary transplant assays to evaluate long-term HSC activity for both the fresh and the cultured HSC transplants (**Figures S3J-M**). In both settings, *Runx2*-deficient donor chimerism remained 2-5-fold higher than the *Runx2*-wt controls. We conclude that even partial loss of *Runx2* is sufficient to significantly boost HSC expansion and long-term repopulation capacity.

Loss of Runx2 causes context-specific transcriptional dysregulation

To characterize the molecular activity of RUNX2 in HSCs, we identified RUNX2 genomic binding using CUT&Tag in day-14 *Runx2*-wt CD201^{+}CD150^{+}KSL pHSCs, and profiled histone H3 lysine 3 trimethylation (H3K4me3) to annotate active gene promoters. We also performed RNA-sequencing on day-14 *Runx2*-wt, *Runx2*-het KO and *Runx2*-hom KO pHSCs to identify transcriptional changes associated with the loss of *Runx2* (**Figure 4A**).

For our transcriptomic analysis, we initially performed principal component analysis (PCA). This separated *Runx2*-wt, *Runx2*-het, and *Runx2*-hom pHSCs by across PC1, suggesting that *Runx2*-het had an intermediate transcriptional phenotype, consistent with the partial loss of *Runx2* (**Figure S4A**). We next performed differential gene expression analysis for *Runx2*-hom and *Runx2*-het samples, relative to *Runx2*-wt controls (**Figure 4B**). Overlapping differentially expressed genes (DEGs), we identified 119 common DEGs, from 564 DEGs in *Runx2*-hom pHSCs and 610 DEGs in the *Runx2*-het context (**Figure 4C**). This implied that many DEGs are *Runx2* dosage specific (**Figure 4C**). Gene Ontology analysis identified DEGs were enriched for genes associated with inflammation and interferons (**Figure 4D; Figure S4B**), which have been shown to promote HSC cell division[48].

From our CUT&Tag experiments, we identified 15,649 statistically significant RUNX2 binding sites in pHSCs, of which 58% were found gene promoters while 13% were found in distal intergenic regions, and the remaining peaks found within gene loci (**Figure 4E)**. This contrasted with its binding in osteoblasts, where only 20% of RUNX2 peaks have been found at gene promoters[49]. Motif analysis of RUNX2 peaks (filtered by genes expressed in *Runx2*-wt pHSCs) identified the RUNX motif, implying that RUNX2 directly bound these genomic sites (**Figure 4F; Figure S4C**). Suggesting potential RUNX2 binding, ETS factor and KLF factor motifs were identified along with binding motifs for KMT2A, ERF, and TYY1 (**Figure 4F; Figure S4C**).

To further understand the potential direct versus indirect regulation of the DEGs by RUNX2, we integrated our RUNX2 target genes with our DEGs (focusing on *Runx2*-hom DEGs). RUNX2 was found to be enriched in a subset of DEG promoters (**Figure 4G**). Within the *Runx2* locus, we observed RUNX2 enrichment at the *Runx2* promoter as well as several intragenic binding sites, suggesting potential autoregulation (**Figure 4H**). Interestingly, there was a strong peak at H3K4me3 for the proximal promoter in WT HSCs, and no peak at the distal promoter (**Figure 4H**), implying the proximal promoter is preferentially used in HSCs[50,51].

To further characterize the cell-type specific effects of *Runx2* loss, we performed RNA-seq on $CD201^{-}CD150^{-}$KSL pHPCs from *Runx2*-wt, *Runx2*-het KO, and *Runx2*-hom KO day-14 cultures. PCA again distinguished samples based on genotype (**Figure S4D**). Similar to the pHSCs, we identified a subset of common DEGs between the *Runx2*-hom and *Runx2*-het samples, relative to *Runx2*-wt controls; 643 of 2016 *Runx2*-het DEGs and 1095 *Runx2*-hom DEGs (**Figure S4E**). While Gene Ontology analysis also identified similar gene sets (**Figure S4F**), only 156 *Runx2*-hom DEGs were present in both HPC and HSC settings (**Figure**

S4G). We therefore conclude that RUNX2 has a context-specific and dosage-specific activity in HSPCs.

Loss of Runx2 enhances HSC self-renewal and inhibits T cell commitment

We were next interested to better understand the cellular mechanisms underlying the enhanced HSC expansion in *Runx2*-KO cultures. To investigate this, we evaluated *Runx2*-KO HSCs at the clonal level over 14-day cultures (**Figure 5A**). Overall clone size was similar between *Runx2*-wt and *Runx2*-hom KO HSCs (**Figure 5B**), and the frequency of clone survival was also similar (**Figure S5A**). However, we observed a significant increase in the number of $CD201^{+}$KSL pHSCs being generated from *Runx2*-hom KO HSC clones (**Figure 5C**). We also identified an increased proportion of HSC clones with high pHSC frequencies (>76%) from *Runx2*-hom KO HSCs (**Figure 5D**). These results suggested that loss of *Runx2* enhances HSC self-renewal divisions, rather than growth or survival. We therefore conclude that *Runx2* regulates HSC cell fate decision.

Finally, we sought to better understand the role of *Runx2* in T-cell development. As described above, *Runx2-KO* HSCs displayed reduced T-cell chimerism in transplantation assays (**Figure 2** and **Figure 3**). This could have been due to a failure of the *Runx2*-KO HSCs to generate T-cells, and/or a failure of the *Runx2-KO* T-cells to survive or proliferate. Intriguingly, several pathways related to T-cell differentiation and activity were identified in our *Runx2*-KO downregulated DEGs (**Figure S4F**), supporting the idea that loss of *Runx2* may alter T cell commitment from HSPCs.

To directly test this hypothesis, we performed *ex vivo* T-cell differentiation assays on 14-day HSPC cultures (**Figure 5E**). T-cell commitment initiates with the stepwise progression through several double negative (DN) cell stages[52], which are discriminated by CD44 and CD25 expression (**Figure 5F; Figure S5B**). We observed a significant, albeit incomplete, reduction in DN2 and DN3-stage T-cell precursors in 7-day cultures, suggesting a DN1-stage block in T-cell commitment (**Figure 5G**). Consistent with this, we also observed a significant reduction in $CD90.2^{+}CD25^{+}$ T-cell precursors (**Figure S5C**). Further discrimination of the DN1 population, using c-Kit and CD24 expression[53], identified a modest but significant build-up of $c\text{-}Kit^{+}CD24^{-}$ and $c\text{-}Kit^{+}CD24^{lo}$ DN1 cells (**Figure S5D**). These results suggest that loss of *Runx2* partially blocks T-cell commitment at an early DN1 cell stage.

To investigate this T-cell commitment in vivo, we evaluated early thymic reconstitution at 4-weeks post-transplantation (**Figure 5H**). We observed a ~2-fold increase in the frequency of *Runx2*-deficient DN1 cells as compared to *Runx2*-wt controls (**Figure 5I; Figure S5E**), in

line with the DN1 stage *ex vivo* phenotype. However, we did not observe a significant difference in the later stages, perhaps due to the different timepoint of analysis and the homeostatic expansion of these T-cell precursors. Consistent with the role of *Runx2* in pDC development, pDC frequencies were also markedly reduced in the thymus (**Figure S5F**). Within the bone marrow, we observed a significant increase in immunophenotypic multipotent progenitor cells[54] (including $Flt3^{+}CD150^{-}$KSL lymphoid-biased multipotent progenitor cells) and $CD127^{+}$KSL common lymphoid progenitor cells (**Figure 5J; Figure S5G**), suggesting that loss of *Runx2* enhances reconstitution of upstream lymphoid progenitor populations. We therefore conclude that loss of *Runx2* alters T-cell commitment but does not block lymphoid progenitor populations.

Discussion

In this study, we performed a genome-wide CRISPR screening for *ex vivo* HSPC expansion regulators. This screen identified both known and novel putative HSC regulators and may provide a useful resource for those interested in the molecular regulation of HSC activity. We have focused on validating and investigating the biology of one of its novel hits, *Runx2*. However, a number of other negative regulators remain to be investigated.

Through use of CRISPR and a hematopoiesis-specific $Runx2^{flox}$ mouse line, we have validated *Runx2* as a potent negative regulator of HSC expansion *ex vivo* and fitness *in vivo*. Notably, *Runx2*-KO HSCs engrafted at ~5-fold higher levels than controls. Clonal analysis implicated loss of *Runx2* leads to improved HSC self-renewal rather than altering rates of survival or proliferation. These results suggest that temporarily inhibiting RUNX2 function could have therapeutic potential to boost HSC expansion and engraftment in the context of stem cell transplantation. However, further studies are warranted to investigate the molecular role of *Runx2* in HSC fate decisions and human HSCs. Additionally, it would be interesting to evaluate *Runx2*-KO HSCs in a head-to-head competitive assay against wild-type HSCs.

Given the fitness advantage of HSCs following *Runx2* loss, we were surprised to find few *RUNX2* mutations in hematological malignancies (in contrast to the occurrence of *RUNX1* mutations)[55,56]. On the contrary, enforced *RUNX2* expression has been associated with the onset of AML and heterozygous loss predicted to delay leukemic onset in mice[16,18]. *RUNX2* is also highly expressed in high-risk T-acute lymphoblastic leukemia[57] and has a role in its progression[47]. From our results, we hypothesize that RUNX2 inhibitors should display a good therapeutic window in the hematopoietic system. Further evidence for this comes from patients with inherited cleidocranial dysplasia (CCD) who carry autosomal dominant

mutations in *RUNX2*[58]. No significant correlations between CCD and hematological or immunological perturbations have been reported, in line with our analysis of steady-state hematopoiesis in *Runx2*^{flox} *Vav1-iCre* mice. However, further characterization of aged *Runx2*^{flox} *Vav1-iCre* mice is warranted.

Constitutive loss of *Runx2* inhibited T-cell commitment and reduced T-cell reconstitution post-transplantation. Thus, any therapeutic potential of *Runx2* as an approach to boost HSC expansion and engraftment should rely on transient inhibition. It will be important to resolve the molecular role of RUNX2 in this process as well as its interactions with RUNX1 and RUNX3 as both factors are also regulators of lymphoid differentiation[59,60]. Given the overlapping expression and targets of Runx factors, it is interesting that loss of a single Runx factor has such strong effects in T-cell development and HSC expansion.

In summary, we used a genome-wide CRISPR KO screen approach to discover *Runx2* as a negative regulator of *ex vivo* HSC expansion and fitness. In validating this finding, we also uncovered a previously unappreciated role for *Runx2* in T-cell development. This study therefore provides important new insights into the molecular regulation of HSC fitness and T-cell commitment.

Acknowledgments

We thank Kosei Ito for sharing the *Runx2*^{flox} mouse line. The mouse Gouda sgRNA KO library was a kind gift from John Doench, and the pMCB406 plasmid was a kind gift from Michael Bassik. We thank the WIMM Transgenics Facility and WIMM Flow Cytometry Facility for supporting this research. We acknowledge funding from the Kay Kendall Leukaemia Fund, the Wellcome Trust, the Krishnan-Ang Foundation, the UK Medical Research Council, the Leukemia and Lymphoma Society, the John Fell Fund, and the European Hematology Association. T.A.M. is supported by the MRC Molecular Haematology Unit grant MC_UU_00029/6.

Authorship contributions

G.A.M and A.C.W made the figures and wrote the manuscript. G.A.M., M.N., A.S., Y.B., M.L., H.V., L.O., O.B., X.H., E.B., M.V.B., J.B., and A.C.W., performed the experiments. I.H, H.M.K, C.C, and T.M. assisted with data analysis. A.C.W conceived the study. All authors edited the manuscript.

Disclosures of conflict of interest

A.C.W. is a consultant for ImmuneBridge. T.A.M. is a paid consultant for and shareholder in Dark Blue Therapeutics Ltd. The remaining authors declare no competing financial interests.

References

1. Mitchell E, Spencer Chapman M, Williams N, et al. Clonal dynamics of haematopoiesis across the human lifespan. *Nature*. 2022;606(7913):343-350. doi:10.1038/s41586-022-04786-y
2. Wilkinson AC, Igarashi KJ, Nakauchi H. Haematopoietic stem cell self-renewal in vivo and ex vivo. *Nat Rev Genet*. 2020;21(9):541-554. doi:10.1038/s41576-020-0241-0
3. Khaddour K, Hana CK, Mewawalla P. Hematopoietic Stem Cell Transplantation. In: *StatPearls*. StatPearls Publishing; 2022. Accessed July 25, 2022. http://www.ncbi.nlm.nih.gov/books/NBK536951/
4. Wilkinson AC, Ishida R, Kikuchi M, et al. Long-term ex vivo hematopoietic stem cell expansion affords nonconditioned transplantation. *Nature*. 2019;571(7763):117-121. doi:10.1038/s41586-019-1244-x
5. Igarashi KJ, Kucinski I, Chan YY, et al. Physioxia improves the selectivity of hematopoietic stem cell expansion cultures. *Blood Adv*. 2023;7(14):3366-3377. doi:10.1182/bloodadvances.2023009668
6. Che JLC, Bode D, Kucinski I, et al. Identification and characterization of in vitro expanded hematopoietic stem cells. *EMBO Rep*. 2022;23(10):e55502. doi:10.15252/embr.202255502
7. Becker HJ, Ishida R, Wilkinson AC, et al. A Single Cell Cloning Platform for Gene Edited Functional Murine Hematopoietic Stem Cells. Published online 23 March 2022:2022.03.23.485423. doi:10.1101/2022.03.23.485423
8. Khoo HM, Meaker GA, Wilkinson AC. Ex Vivo Expansion and Genetic Manipulation of Mouse Hematopoietic Stem Cells in Polyvinyl Alcohol-Based Cultures. *JoVE J Vis Exp*. 2023;(192):e64791. doi:10.3791/64791
9. Wilkinson AC, Dever DP, Baik R, et al. Cas9-AAV6 gene correction of beta-globin in autologous HSCs improves sickle cell disease erythropoiesis in mice. *Nat Commun*. 2021;12(1):686. doi:10.1038/s41467-021-20909-x
10. Sakurai M, Ishitsuka K, Ito R, et al. Chemically defined cytokine-free expansion of human haematopoietic stem cells. *Nature*. 2023;615(7950):127-133. doi:10.1038/s41586-023-05739-9
11. de Bruijn M, Dzierzak E. Runx transcription factors in the development and function of the definitive hematopoietic system. *Blood*. 2017;129(15):2061-2069. doi:10.1182/blood-2016-12-689109
12. Lacaud G, Gore L, Kennedy M, et al. Runx1 is essential for hematopoietic commitment at the hemangioblast stage of development in vitro. *Blood*. 2002;100(2):458-466. doi:10.1182/blood-2001-12-0321
13. Sood R, Kamikubo Y, Liu P. Role of RUNX1 in hematological malignancies. *Blood*. 2017;129(15):2070-2082. doi:10.1182/blood-2016-10-687830
14. Wang CQ, Motoda L, Satake M, et al. Runx3 deficiency results in myeloproliferative disorder in aged mice. *Blood*. 2013;122(4):562-566. doi:10.1182/blood-2012-10-460618
15. Meng Y, Carrelha J, Drissen R, et al. Epigenetic programming defines haematopoietic stem cell fate restriction. *Nat Cell Biol*. 2023;25(6):812-822. doi:10.1038/s41556-023-01137-5
16. Kuo YH, Zaidi SK, Gornostaeva S, Komori T, Stein GS, Castilla LH. Runx2 induces acute myeloid leukemia in cooperation with Cbfβ-SMMHC in mice. *Blood*. 2009;113(14):3323-3332. doi:10.1182/blood-2008-06-162248

17. Komori T. Regulation of Osteoblast Differentiation by Runx2. In: Choi Y, ed. *Osteoimmunology*. Advances in Experimental Medicine and Biology. Springer US; 2010:43-49. doi:10.1007/978-1-4419-1050-9_5
18. Castilla LH, Perrat P, Martinez NJ, et al. Identification of genes that synergize with Cbfb-MYH11 in the pathogenesis of acute myeloid leukemia. *Proc Natl Acad Sci*. 2004;101(14):4924-4929. doi:10.1073/pnas.0400930101
19. Sawai CM, Sisirak V, Ghosh HS, et al. Transcription factor Runx2 controls the development and migration of plasmacytoid dendritic cells. *J Exp Med*. 2013;210(11):2151-2159. doi:10.1084/jem.20130443
20. Qin X, Jiang Q, Nagano K, et al. Runx2 is essential for the transdifferentiation of chondrocytes into osteoblasts. *PLOS Genet*. 2020;16(11):e1009169. doi:10.1371/journal.pgen.1009169
21. Goodwin LO, Splinter E, Davis TL, et al. Large-scale discovery of mouse transgenic integration sites reveals frequent structural variation and insertional mutagenesis. *Genome Res*. 2019;29(3):494-505. doi:10.1101/gr.233866.117
22. DeWeirdt PC, Sangree AK, Hanna RE, et al. Genetic screens in isogenic mammalian cell lines without single cell cloning. *Nat Commun*. 2020;11:752. doi:10.1038/s41467-020-14620-6
23. Haney MS, Shankar A, Olender L, et al. In vivo CRISPR screening identifies SAGA complex members as key regulators of hematopoiesis. Published online 19 May 2025:2022.07.22.501030. doi:10.1101/2022.07.22.501030
24. Li W, Xu H, Xiao T, et al. MAGeCK enables robust identification of essential genes from genome-scale CRISPR/Cas9 knockout screens. *Genome Biol*. 2014;15(12):554. doi:10.1186/s13059-014-0554-4
25. Morgens DW, Wainberg M, Boyle EA, et al. Genome-scale measurement of off-target activity using Cas9 toxicity in high-throughput screens. *Nat Commun*. 2017;8:15178. doi:10.1038/ncomms15178
26. Hodgkins A, Farne A, Perera S, et al. WGE: a CRISPR database for genome engineering. *Bioinformatics*. 2015;31(18):3078-3080. doi:10.1093/bioinformatics/btv308
27. Kaya-Okur HS, Wu SJ, Codomo CA, et al. CUT&Tag for efficient epigenomic profiling of small samples and single cells. *Nat Commun*. 2019;10(1):1930. doi:10.1038/s41467-019-09982-5
28. Andrews S. FastQC, https://www.bioinformatics.babraham.ac.uk/projects/fastqc/. Published online 2010. https://www.bioinformatics.babraham.ac.uk/projects/fastqc/
29. Krueger F. Trim Galore, https://www.bioinformatics.babraham.ac.uk/projects/trim_galore/. Published online 2012.
30. Langmead B, Salzberg SL. Fast gapped-read alignment with Bowtie 2. *Nat Methods*. 2012;9(4):357-359. doi:10.1038/nmeth.1923
31. Ramírez F, Ryan DP, Grüning B, et al. deepTools2: a next generation web server for deep-sequencing data analysis. *Nucleic Acids Res*. 2016;44(Web Server issue):W160-W165. doi:10.1093/nar/gkw257
32. Hentges LD, Sergeant MJ, Cole CB, Downes DJ, Hughes JR, Taylor S. LanceOtron: a deep learning peak caller for genome sequencing experiments. *Bioinformatics*. 2022;38(18):4255-4263. doi:10.1093/bioinformatics/btac525
33. Bailey TL. STREME: accurate and versatile sequence motif discovery. *Bioinformatics*. 2021;37(18):2834-2840. doi:10.1093/bioinformatics/btab203
34. Gupta S, Stamatoyannopoulos JA, Bailey TL, Noble WS. Quantifying similarity between motifs. *Genome Biol*. 2007;8(2):R24. doi:10.1186/gb-2007-8-2-r24
35. Dobin A, Davis CA, Schlesinger F, et al. STAR: ultrafast universal RNA-seq aligner. *Bioinformatics*. 2013;29(1):15-21. doi:10.1093/bioinformatics/bts635
36. Liao Y, Smyth GK, Shi W. featureCounts: an efficient general purpose program for assigning sequence reads to genomic features. *Bioinformatics*. 2014;30(7):923-930. doi:10.1093/bioinformatics/btt656

37. Love MI, Huber W, Anders S. Moderated estimation of fold change and dispersion for RNA-seq data with DESeq2. *Genome Biol*. 2014;15(12):550. doi:10.1186/s13059-014-0550-8
38. Yu G, Wang LG, Han Y, He QY. clusterProfiler: an R Package for Comparing Biological Themes Among Gene Clusters. *OMICS J Integr Biol*. 2012;16(5):284-287. doi:10.1089/omi.2011.0118
39. Dempster JM, Rossen J, Kazachkova M, et al. Extracting Biological Insights from the Project Achilles Genome-Scale CRISPR Screens in Cancer Cell Lines. Published online 31 July 2019:720243. doi:10.1101/720243
40. Pimanda JE, Ottersbach K, Knezevic K, et al. Gata2, Fli1, and Scl form a recursively wired gene-regulatory circuit during early hematopoietic development. *Proc Natl Acad Sci U S A*. 2007;104(45):17692-17697. doi:10.1073/pnas.0707045104
41. Wilkinson AC, Göttgens B. Transcriptional Regulation of Haematopoietic Stem Cells. In: Hime G, Abud H, eds. *Transcriptional and Translational Regulation of Stem Cells*. Springer Netherlands; 2013:187-212. doi:10.1007/978-94-007-6621-1_11
42. Yamada Y, Warren AJ, Dobson C, Forster A, Pannell R, Rabbitts TH. The T cell leukemia LIM protein Lmo2 is necessary for adult mouse hematopoiesis. *Proc Natl Acad Sci U S A*. 1998;95(7):3890-3895.
43. Abbas HA, Pant V, Lozano G. The ups and downs of p53 regulation in hematopoietic stem cells. *Cell Cycle*. 2011;10(19):3257-3262. doi:10.4161/cc.10.19.17721
44. Zhang J, Grindley JC, Yin T, et al. PTEN maintains haematopoietic stem cells and acts in lineage choice and leukaemia prevention. *Nature*. 2006;441(7092):518-522. doi:10.1038/nature04747
45. Szklarczyk D, Kirsch R, Koutrouli M, et al. The STRING database in 2023: protein–protein association networks and functional enrichment analyses for any sequenced genome of interest. *Nucleic Acids Res*. 2022;51(D1):D638-D646. doi:10.1093/nar/gkac1000
46. Becker HJ, Ishida R, Wilkinson AC, et al. Controlling genetic heterogeneity in gene-edited hematopoietic stem cells by single-cell expansion. *Cell Stem Cell*. 2023;30(7):987-1000.e8. doi:10.1016/j.stem.2023.06.002
47. Matthijssens F, Sharma ND, Nysus M, et al. RUNX2 regulates leukemic cell metabolism and chemotaxis in high-risk T cell acute lymphoblastic leukemia. *J Clin Invest*. 2021;131(6). doi:10.1172/JCI141566
48. Essers MAG, Offner S, Blanco-Bose WE, et al. IFNα activates dormant haematopoietic stem cells in vivo. *Nature*. 2009;458(7240):904-908. doi:10.1038/nature07815
49. Wu H, Whitfield TW, Gordon JAR, et al. Genomic occupancy of Runx2 with global expression profiling identifies a novel dimension to control of osteoblastogenesis. *Genome Biol*. 2014;15(3):R52. doi:10.1186/gb-2014-15-3-r52
50. Xiao ZS, Liu SG, Hinson TK, Quarles LD. Characterization of the upstream mouse Cbfa1/Runx2 promoter. *J Cell Biochem*. 2001;82(4):647-659. doi:10.1002/jcb.1192
51. Xiao ZS, Thomas R, Hinson TK, Quarles LD. Genomic structure and isoform expression of the mouse, rat and human *Cbfa1/Osf2* transcription factor1. *Gene*. 1998;214(1):187-197. doi:10.1016/S0378-1119(98)00227-3
52. Famili F, Wiekmeijer AS, Staal FJ. The Development of T Cells From Stem Cells in Mice and Humans. *Future Sci OA*. 2017;3(3):FSO186. doi:10.4155/fsoa-2016-0095
53. Porritt HE, Rumfelt LL, Tabrizifard S, Schmitt TM, Zúñiga-Pflücker JC, Petrie HT. Heterogeneity among DN1 prothymocytes reveals multiple progenitors with different capacities to generate T cell and non-T cell lineages. *Immunity*. 2004;20(6):735-745. doi:10.1016/j.immuni.2004.05.004
54. Challen GA, Pietras EM, Wallscheid NC, Signer RAJ. Simplified murine multipotent progenitor isolation scheme: Establishing a consensus approach for multipotent progenitor identification. *Exp Hematol*. 2021;104:55-63. doi:10.1016/j.exphem.2021.09.007
55. Blyth K, Cameron ER, Neil JC. The runx genes: gain or loss of function in cancer. *Nat Rev Cancer*. 2005;5(5):376-387. doi:10.1038/nrc1607

56. Blyth K, Vaillant F, Jenkins A, et al. Runx2 in normal tissues and cancer cells: A developing story. *Blood Cells Mol Dis*. 2010;45(2):117-123. doi:10.1016/j.bcmd.2010.05.007
57. Sharma ND, Nickl CC, Kang H, et al. RUNX2 Regulates Cell Migration in T-Cell Lineage Acute Lymphoblastic Leukemia. *Blood*. 2019;134(Supplement_1):3947. doi:10.1182/blood-2019-129337
58. Jaruga A, Hordyjewska E, Kandzierski G, Tylzanowski P. Cleidocranial dysplasia and RUNX2-clinical phenotype–genotype correlation. *Clin Genet*. 2016;90(5):393-402. doi:10.1111/cge.12812
59. Shin B, Hosokawa H, Romero-Wolf M, et al. Runx1 and Runx3 drive progenitor to T-lineage transcriptome conversion in mouse T cell commitment via dynamic genomic site switching. *Proc Natl Acad Sci U S A*. 2021;118(4):e2019655118. doi:10.1073/pnas.2019655118
60. Shin B, Zhou W, Wang J, Gao F, Rothenberg EV. Runx factors launch T cell and innate lymphoid programs via direct and gene network-based mechanisms. *Nat Immunol*. 2023;24(9):1458-1472. doi:10.1038/s41590-023-01585-z

Figures legends

Figure 1: Genome-wide ex vivo HSPC CRISPR screen identifies putative regulators of expansion

(A) Schematic overview of *ex vivo* HSPC CRISPR KO screen for top putative negative regulators. Created in BioRender.

(B) Beta-score for the 21,601 genes targeted in the *ex vivo* HSPC expansion screen. Inset: Top 20 beta-score genes listed within insert.

(C) Venn diagram of the overlap in essential genes from Achilles common essential list[31] and the essential genes identified in our HSPC screen.

(D) STRING analysis of protein-protein interactions of genes with positive beta value and FDR < 10%. Thicker line = stronger reported interaction. Interactions can be: from curated databases, experimentally determined, gene neighbourhood, gene fusions, gene co-occurrence, textmining, co-expression and protein homology.

(E) Time course of sgRNA-expressing cells over time for the three *Runx* genes and control gRNAs, normalised to t0. FDR and p-values from the screen analysis shown above.

Figure 2: CRISPR-mediated KO of Runx2 enhances HSC expansion and engraftment

(A) Schematic of *Runx2*-targeting sgRNAs.

(B) Schematic overview of the experiment. Two guides targeting *Runx2* and two control guides (one non-targeting and one targeting the safe harbour locus *Rosa26*) were used. Created in BioRender.

(C) Intracellular flow cytometric analysis for RUNX2 in control and *Runx2*-KO HSPC cultures. n = 3.

(D) Representative flow cytometry plots showing differences in pHSC ($CD201^+CD150^+cKit^+Sca1^+Lineage^-$) populations *ex vivo* in *Runx2*-KO and control HSPC cultures.

(E) *Ex vivo* pHSC frequency at 21 days. See **Figure S2C** for data for days 0-14. Data normalised to controls. n = 4.

(F) Experimental overview of competitive transplant assay following *ex vivo* culture of $cKit^+$ cells from C57BL/6-Gt(ROSA)26Sor$^{tm1(rtTA*M2)Jae}$ Col1a1$^{tm1(tetO\text{-}cas9)Sho}$ doxycycline-inducible Cas9 mice. 2000 donor $CD45.2^+$ pHSCs alongside 1 million $CD45.1^+CD45.2^+$ whole bone marrow cells were transplanted into lethally irradiated $CD45.1^+$ recipient mice. Created in BioRender.

(G) Peripheral blood donor chimerism over 20 weeks following transplantation. n = 10. 2-way ANOVA was performed.

(H) Donor chimerism within peripheral blood myeloid, T and B cell compartments at the 20-week endpoint. 2-way ANOVA was performed.

(I) Bone marrow donor chimerism at the 20-week transplant endpoint. n = 10. 2-way ANOVA was performed.

(J) Proportion of myeloid, B and T cells within the $CD45.2^+$ donor peripheral blood cell compartment at the 20-week endpoint. n = 10. 2-way ANOVA was performed.

Non-significance not labelled.

Figure 3: Heterozygous loss of Runx2 is sufficient to drive increased HSC expansion and reconstitution potentials

(A) Experimental overview for assays exploring the phenotypes of homozygous and heterozygous *Runx2* KO HSCs. Created in BioRender.

(B) Peripheral blood chimerism from transplantation assays using 100 fresh $CD45.2^+$ HSCs vs 0.5 million $CD45.1^+CD45.2^+$ WBM competitor cells. n = 3-5. 2-way ANOVA was performed.

(C) Donor chimerism within whole bone marrow (WBM), spleen, thymus and peripheral blood (PB) chimerism of competitive transplant assay using 100 fresh $CD45.2^+$ HSCs. n = 3-5. 2-way ANOVA was performed.

(D) 16-week peripheral blood lineage output of competitive transplant assay using 100 fresh sorted $CD45.2^+$ HSCs. n = 3-5. 2-way ANOVA was performed.

(E) *Ex vivo* pHSC frequency over three-week culture. n = 6.

(F) Peripheral blood chimerism from transplantation assays using 10,000 $CD45.2^+$ cultured HSPCs vs 1 million $CD45.1^+CD45.2^+$ WBM competitor cells. n = 3-4. 2-way ANOVA was performed.

(G) Donor chimerism within WBM, spleen, thymus and PB from transplantation assays using 10,000 $CD45.2^+$ 14-day cultured HSPCs. n = 3-4. 2-way ANOVA was performed.

(H) 16-week peripheral blood lineage output of competitive transplant assay using 10,000 $CD45.2^+$ 14-day cultured HSPCs. n = 3-4. 2-way ANOVA was performed.

Non-significance not labelled.

Figure 4: Loss of Runx2 causes context-specific transcriptional changes

(A) Experimental overview for RNA-seq and CUT&Tag on cultured pHSCs ($CD201^+CD150^+$KSL). Created in BioRender.

(B) Volcano plot of differentially expressed genes (DEGs) for *Runx2*-het KO vs *Runx2*-wt (left plot) and *Runx2*-hom KO vs *Runx2*-wt (right plot) in pHSCs.

(C) Gene overlap for *Runx2*-hom KO vs *Runx2*-wt DEGs and *Runx2*-het KO vs *Runx2*-wt DEGs in pHSCs (for DEGs with adjusted $p<0.05$).

(D) Top 30 upregulated Gene Ontology Biological Process for *Runx2*-hom KO vs *Runx2*-wt pHSC RNA-seq.

(E) Genomic features present at RUNX2 peaks in *Runx2-wt* pHSCs.

(F) Top 6 motifs present in RUNX2-bound promoters after filtered by genes expressed in *Runx2*-wt pHSC RNA-seq. p-value calculated using a null model consisting of sampling motif columns from all the columns in the set of target motifs.

(G) RUNX2 binding across promoters in DEGs from *Runx2*-hom KO vs *Runx2*-wt pHSC RNA-seq.

(H) Genome track of the *Runx2* gene locus showing RUNX2 and H3K4me3 CUT&Tag in *Runx2*-wt pHSCs.

Figure 5: Loss of Runx2 enhances HSC self-renewal but decreases T-cell commitment

(A) Experimental overview for *ex vivo* clonal plating assays of *Runx2*-hom KO HSCs. Created in BioRender.

(B) Number of live cells per positive well 14 days after single cell plating of $CD201^+CD150^+KSL$, analysed via one-way ANOVA. n = 190. Numbers above data indicate number of positive wells for each genotype. Line at median with 95% CI. Unpaired T-test was performed.

(C) Number of $CD201^+KSL$ live cells in wells 14 days after single cell plating of $CD201^+CD150^+KSL$, analysed via 1-way ANOVA. n = 190. Numbers below data indicate number of positive wells for each genotype. Line at median with 95% CI. Unpaired T-test was performed.

(D) Clonal identities at 14-days after single cell plating and percentage of wells with this identity. Low output clones = 5-50% $CD201^+KSL$, Medium output clones = 50-75% $CD201^+KSL$, High output clones = > 75% $CD201^+KSL$.

(E) Experimental overview for *ex vivo* T-cell differentiation assays of *Runx2*-hom HSCs. Created in BioRender.

(F) Representative flow plot of *ex vivo* T-cell differentiation generating DN1 to DN3 stages after 7-days.

(G) Frequency of DN1 to DN3 stage cells generated in *ex vivo* T-cell differentiation assays. n = 7, unpaired T-test was performed.

(H) Experimental overview for 4-week competitive transplantation assay. Created in BioRender.

(I) Frequency of DN1 to DN3 stage cells in $CD45.2^+$ donor derived $CD8^-CD8^-$ cells in the thymus of recipient mice at 4-week endpoint. n = 5, unpaired T-test was performed.

(J) Frequency of immunophenotypic HSPC populations in donor derived bone marrow of recipient mice at 4-week endpoint. n = 5, unpaired T-test was performed. HSC = $CD150^{+}CD48^{-}KSL$, MPP = $CD150^{-}CD48^{-}Flt3^{-}KSL$, $MPP^{G/M}$ = $CD150^{+}CD48^{-}Flt3^{-}KSL$, $MPP^{Mk/E}$ = $CD150^{+}CD48^{+}Flt3^{-}KSL$, MPP^{Ly} = $CD150^{-}Flt3^{+}KSL$, CLP = $CD127^{+}KSL$.

Non-significance not labelled.

Figure 1

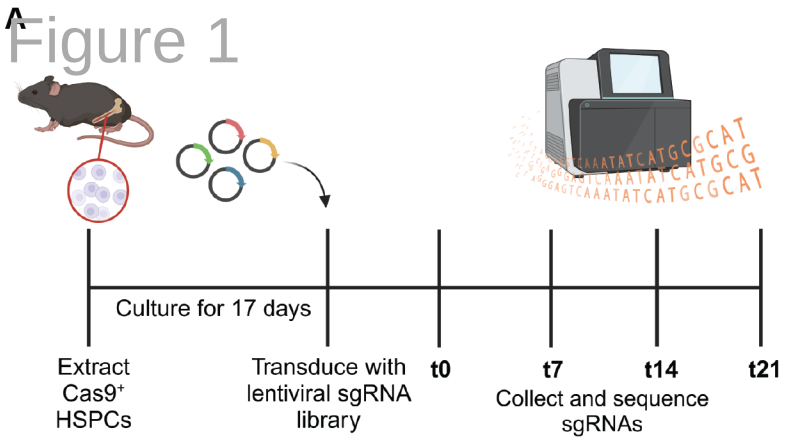
A
Culture for 17 days
Extract Cas9+ HSPCs
Transduce with lentiviral sgRNA library
t0
t7
t14
t21
Collect and sequence sgRNAs

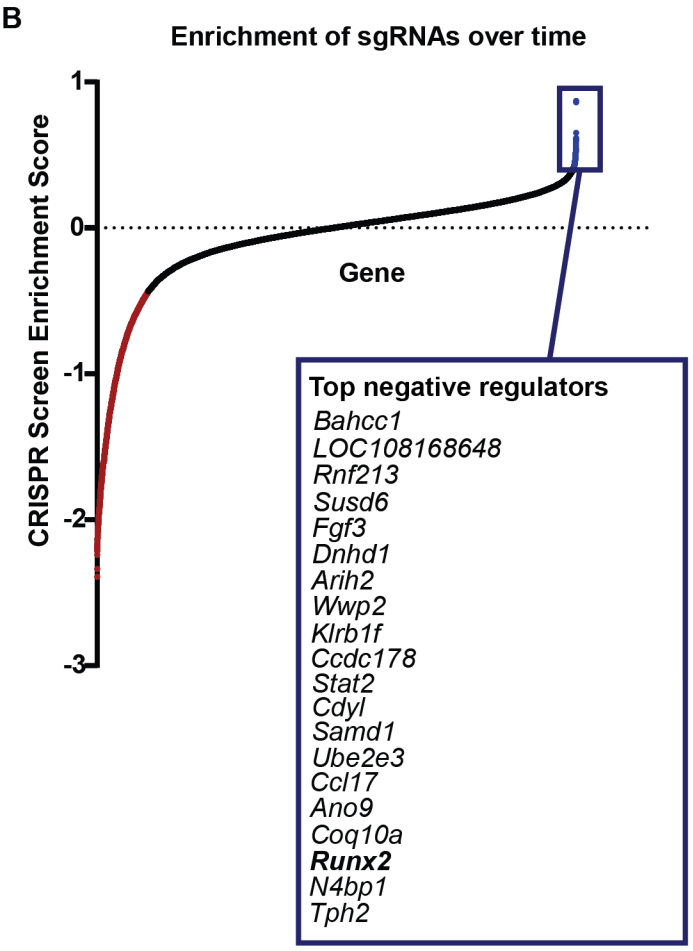
B
Enrichment of sgRNAs over time
CRISPR Screen Enrichment Score
Gene
Top negative regulators
Bahcc1
LOC108168648
Rnf213
Susd6
Fgf3
Dnhd1
Arih2
Wwp2
Klrb1f
Ccdc178
Stat2
Cdyl
Samd1
Ube2e3
Ccl17
Ano9
Coq10a
Runx2
N4bp1
Tph2

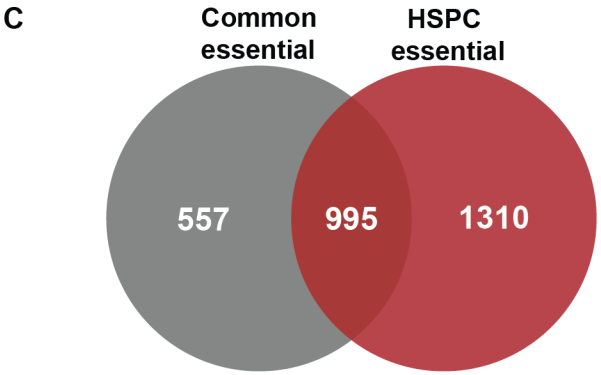
C
Common essential
HSPC essential
557
995
1310

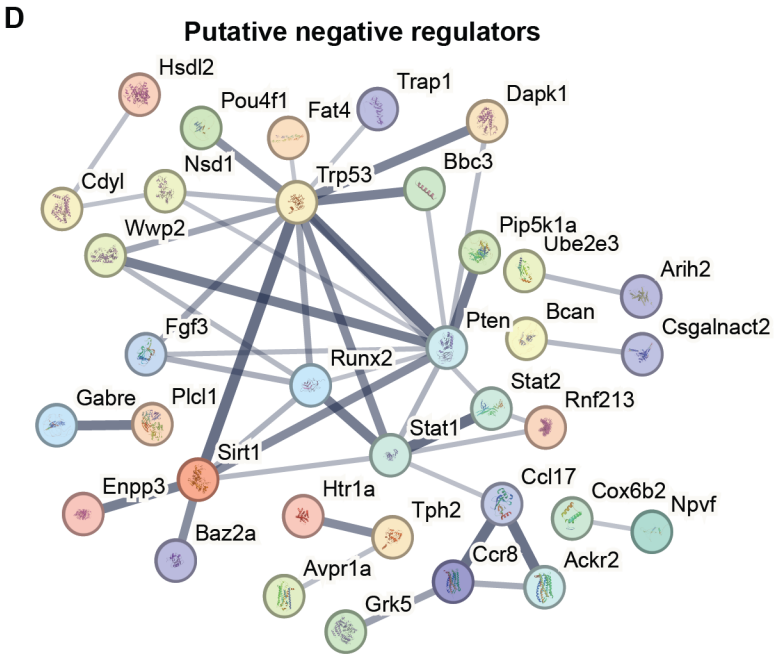
D
Putative negative regulators
Hsdl2
Pou4f1
Fat4
Trap1
Dapk1
Cdyl
Nsd1
Trp53
Bbc3
Wwp2
Pip5k1a
Ube2e3
Arih2
Fgf3
Pten
Bcan
Csgalnact2
Runx2
Stat2
Rnf213
Gabre
Plcl1
Stat1
Sirt1
Ccl17
Cox6b2
Npvf
Enpp3
Htr1a
Tph2
Baz2a
Ccr8
Ackr2
Avpr1a
Grk5

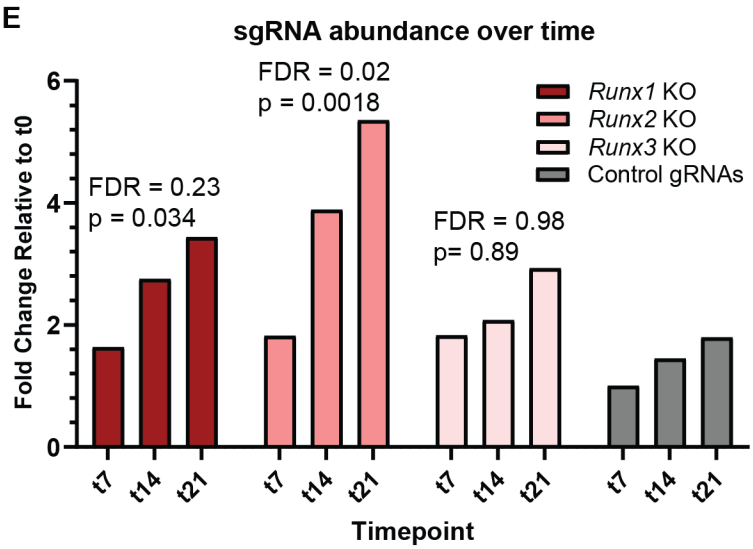
E
sgRNA abundance over time
Fold Change Relative to t0
FDR = 0.23
p = 0.034
FDR = 0.02
p = 0.0018
FDR = 0.98
p= 0.89
Runx1 KO
Runx2 KO
Runx3 KO
Control gRNAs
t7
t14
t21
Timepoint

Figure 2

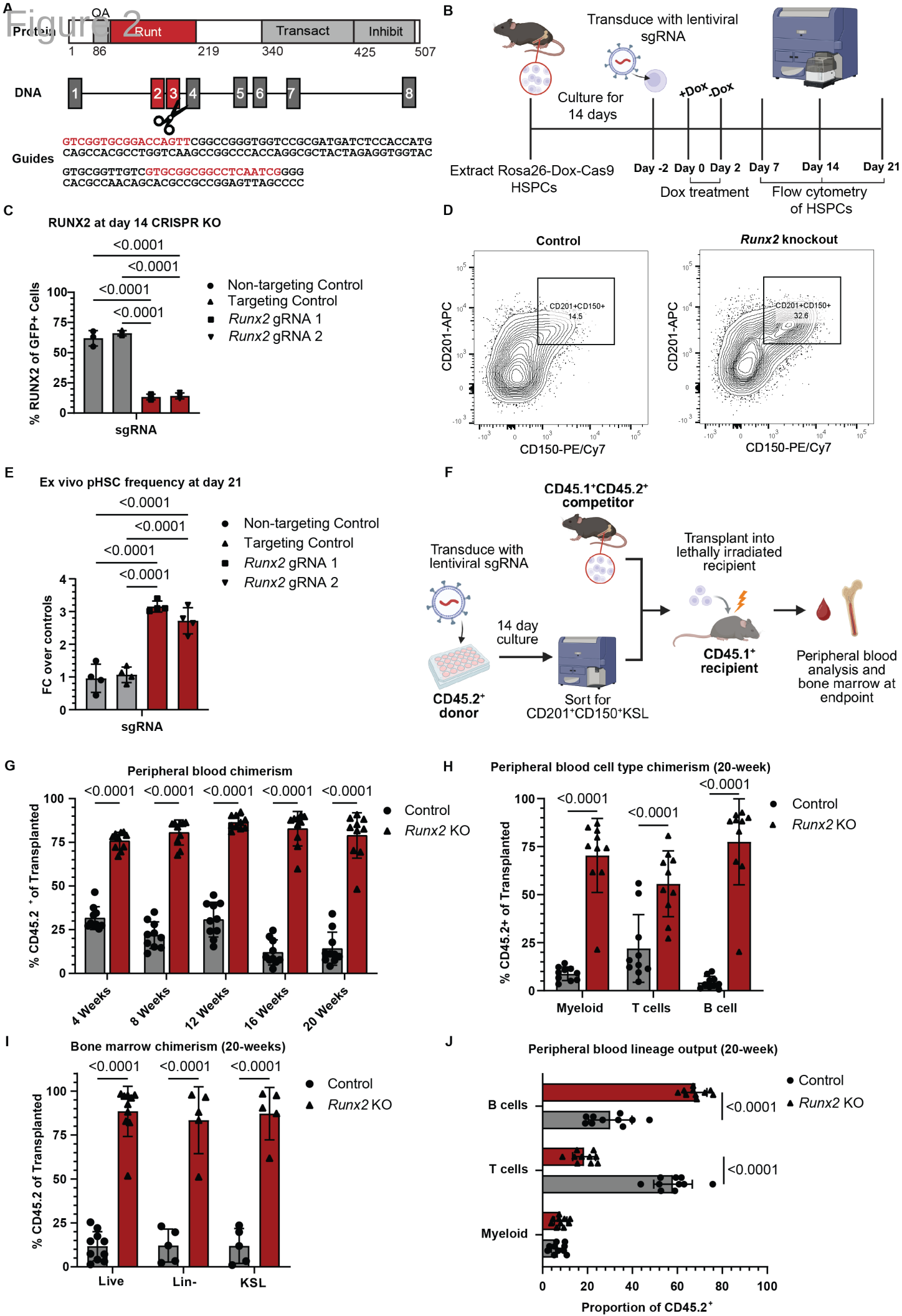
A
Protein
QA
Runt
Transact
Inhibit
1
86
219
340
425
507
DNA
1
2
3
4
5
6
7
8
Guides
GTCGGTGCGGACCAGTTCGGCCGGGTGGTCCGCGATGATCTCCACCATG
CAGCCACGCCTGGTCAAGCCGGCCCACCAGGCGCTACTAGAGGTGGTAC
GTGCGGTTGTCGTGCGGCGGCCTCAATCGGGG
CACGCCAACAGCACGCCGCCGGAGTTAGCCCC
B
Transduce with lentiviral sgRNA
Culture for 14 days
+Dox
-Dox
Extract Rosa26-Dox-Cas9 HSPCs
Day -2
Day 0
Day 2
Day 7
Day 14
Day 21
Dox treatment
Flow cytometry of HSPCs
C
RUNX2 at day 14 CRISPR KO
<0.0001
<0.0001
<0.0001
<0.0001
% RUNX2 of GFP+ Cells
sgRNA
Non-targeting Control
Targeting Control
Runx2 gRNA 1
Runx2 gRNA 2
D
Control
Runx2 knockout
CD201+CD150+
14.5
32.6
CD201-APC
CD150-PE/Cy7
E
Ex vivo pHSC frequency at day 21
<0.0001
<0.0001
<0.0001
<0.0001
FC over controls
sgRNA
Non-targeting Control
Targeting Control
Runx2 gRNA 1
Runx2 gRNA 2
F
CD45.1+CD45.2+ competitor
Transduce with lentiviral sgRNA
14 day culture
CD45.2+ donor
Sort for CD201+CD150+KSL
Transplant into lethally irradiated recipient
CD45.1+ recipient
Peripheral blood analysis and bone marrow at endpoint
G
Peripheral blood chimerism
<0.0001
<0.0001
<0.0001
<0.0001
<0.0001
% CD45.2 + of Transplanted
4 Weeks
8 Weeks
12 Weeks
16 Weeks
20 Weeks
Control
Runx2 KO
H
Peripheral blood cell type chimerism (20-week)
<0.0001
<0.0001
<0.0001
% CD45.2+ of Transplanted
Myeloid
T cells
B cell
Control
Runx2 KO
I
Bone marrow chimerism (20-weeks)
<0.0001
<0.0001
<0.0001
% CD45.2 of Transplanted
Live
Lin-
KSL
Control
Runx2 KO
J
Peripheral blood lineage output (20-week)
B cells
T cells
Myeloid
<0.0001
<0.0001
0
20
40
60
80
100
Proportion of CD45.2+
Control
Runx2 KO

Figure 3

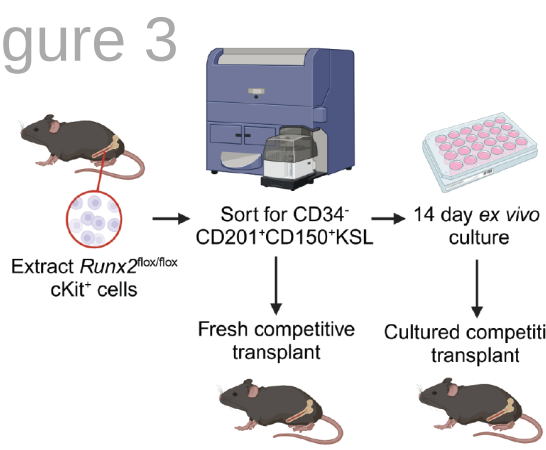
A
Extract Runx2flox/flox cKit+ cells
Sort for CD34- CD201+CD150+KSL
14 day ex vivo culture
Fresh competitive transplant
Cultured competitive transplant

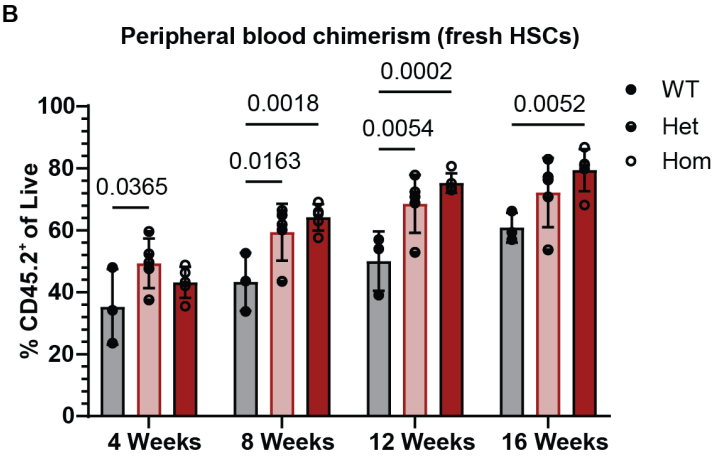
B
Peripheral blood chimerism (fresh HSCs)
% CD45.2+ of Live
0.0365
0.0163
0.0018
0.0054
0.0002
0.0052
4 Weeks
8 Weeks
12 Weeks
16 Weeks
WT
Het
Hom

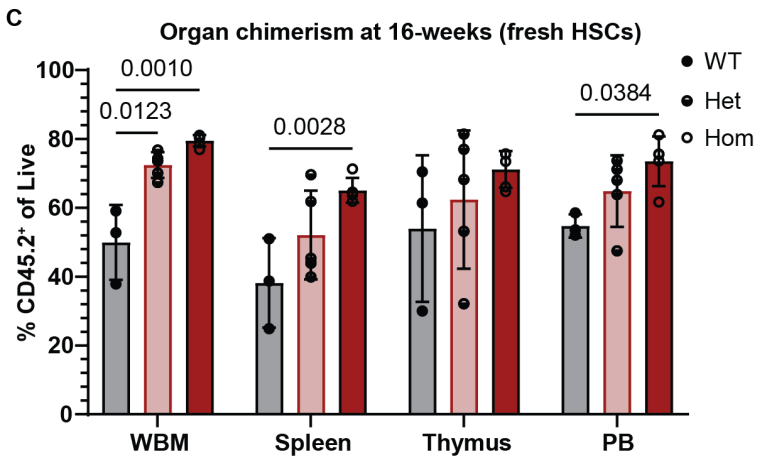
C
Organ chimerism at 16-weeks (fresh HSCs)
% CD45.2+ of Live
0.0010
0.0123
0.0028
0.0384
WBM
Spleen
Thymus
PB
WT
Het
Hom

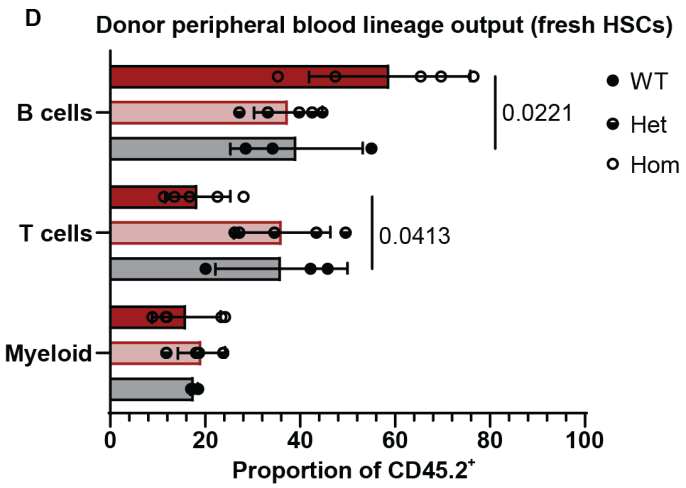
D
Donor peripheral blood lineage output (fresh HSCs)
B cells
T cells
Myeloid
0.0221
0.0413
Proportion of CD45.2+
WT
Het
Hom

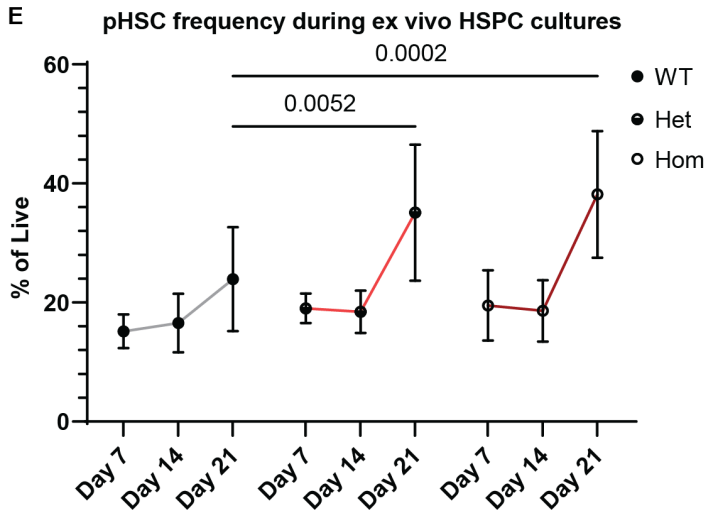
E
pHSC frequency during ex vivo HSPC cultures
% of Live
0.0002
0.0052
Day 7
Day 14
Day 21
WT
Het
Hom

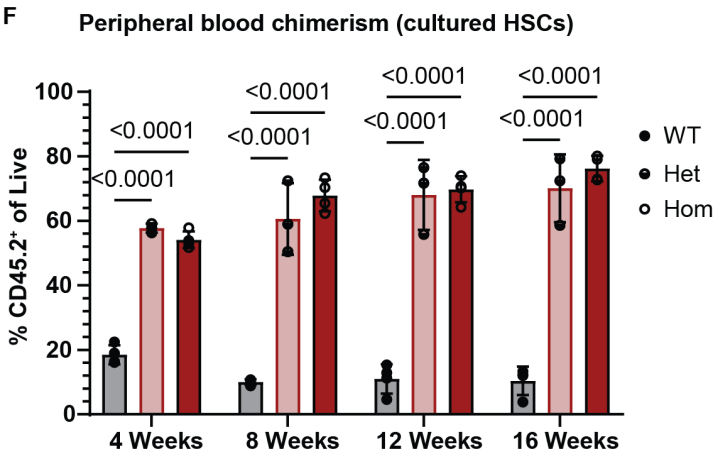
F
Peripheral blood chimerism (cultured HSCs)
% CD45.2+ of Live
<0.0001
4 Weeks
8 Weeks
12 Weeks
16 Weeks
WT
Het
Hom

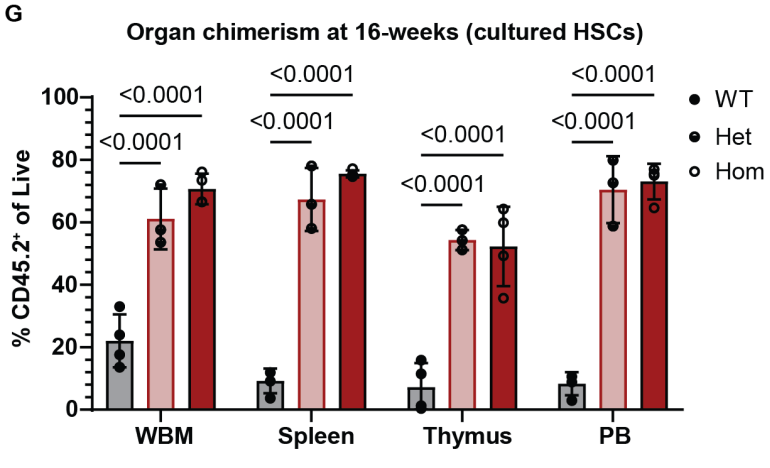
G
Organ chimerism at 16-weeks (cultured HSCs)
% CD45.2+ of Live
<0.0001
WBM
Spleen
Thymus
PB
WT
Het
Hom

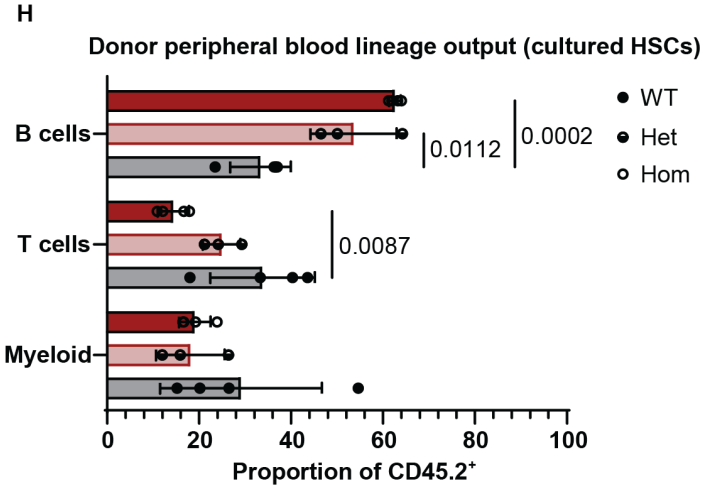
H
Donor peripheral blood lineage output (cultured HSCs)
B cells
T cells
Myeloid
0.0112
0.0002
0.0087
Proportion of CD45.2+
WT
Het
Hom

Figure 4


A
Extract Runx2flox/flox cKit+ cells
14 day ex vivo culture
Sort CD201+CD150+KSL for RNA-seq and CUT&TAG

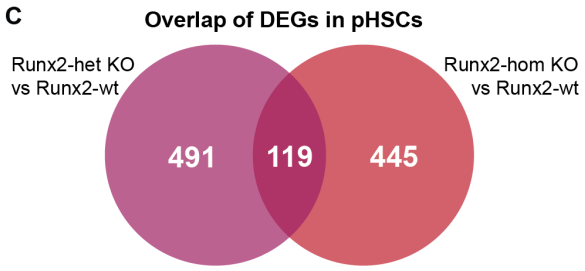
C
Overlap of DEGs in pHSCs
Runx2-het KO vs Runx2-wt
Runx2-hom KO vs Runx2-wt
491
119
445


B
Runx2-het KO vs Runx2-wt
DEGs
Down
NotSig
Up
−log10 adjusted p−value
log2 fold change
Commd10
Dok3
Apoe
Ifi27
H2−Ob
Runx2
Dusp6
Skil
Septin11
Hells

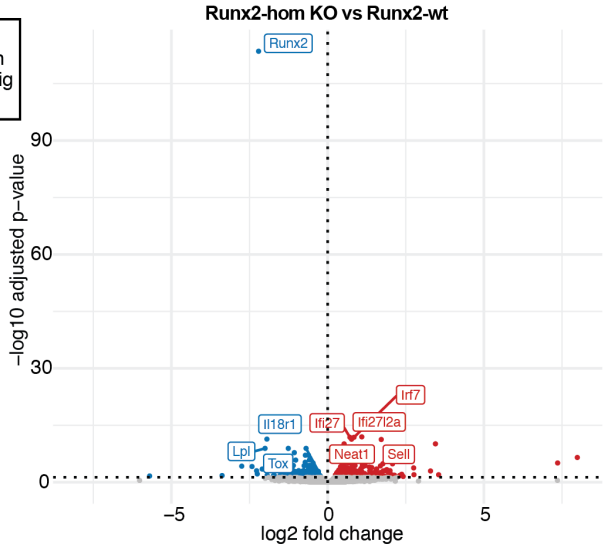
Runx2-hom KO vs Runx2-wt
−log10 adjusted p−value
log2 fold change
Runx2
Irf7
Il18r1
Ifi27
Ifi27l2a
Lpl
Tox
Neat1
Sell

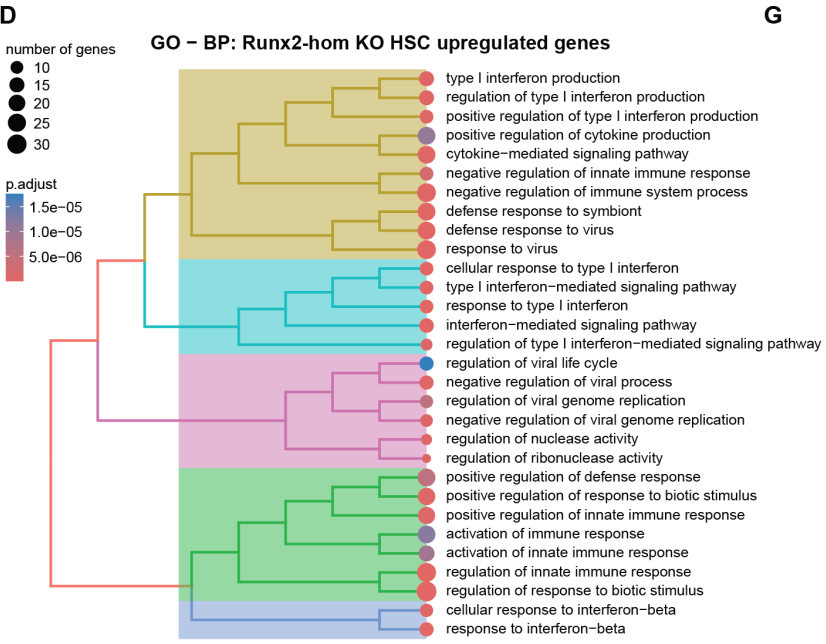
D
GO − BP: Runx2-hom KO HSC upregulated genes
number of genes
10
15
20
25
30
p.adjust
1.5e−05
1.0e−05
5.0e−06
type I interferon production
regulation of type I interferon production
positive regulation of type I interferon production
positive regulation of cytokine production
cytokine−mediated signaling pathway
negative regulation of innate immune response
negative regulation of immune system process
defense response to symbiont
defense response to virus
response to virus
cellular response to type I interferon
type I interferon−mediated signaling pathway
response to type I interferon
interferon−mediated signaling pathway
regulation of type I interferon−mediated signaling pathway
regulation of viral life cycle
negative regulation of viral process
regulation of viral genome replication
negative regulation of viral genome replication
regulation of nuclease activity
regulation of ribonuclease activity
positive regulation of defense response
positive regulation of response to biotic stimulus
positive regulation of innate immune response
activation of immune response
activation of innate immune response
regulation of innate immune response
regulation of response to biotic stimulus
cellular response to interferon−beta
response to interferon−beta

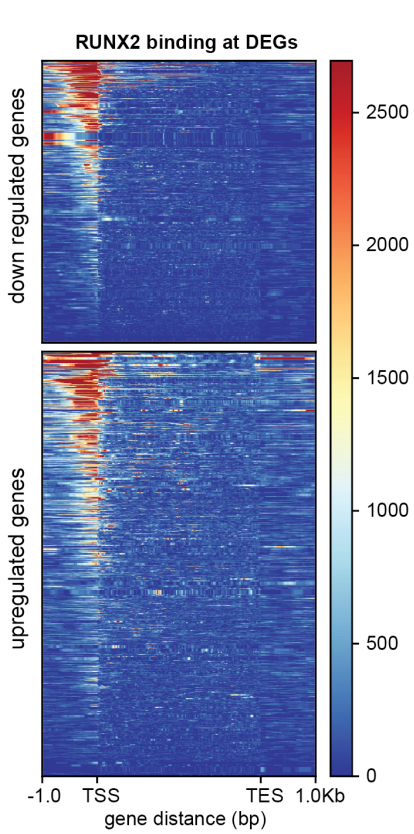
G
RUNX2 binding at DEGs
down regulated genes
upregulated genes
2500
2000
1500
1000
500
0
-1.0
TSS
TES
1.0Kb
gene distance (bp)

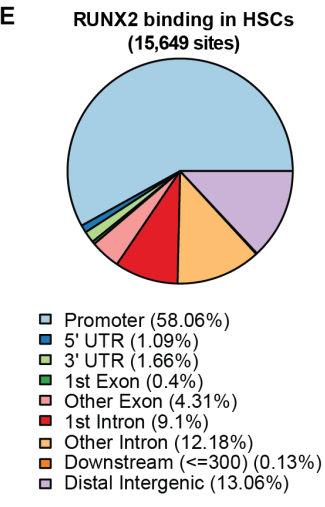
E
RUNX2 binding in HSCs
(15,649 sites)
Promoter (58.06%)
5' UTR (1.09%)
3' UTR (1.66%)
1st Exon (0.4%)
Other Exon (4.31%)
1st Intron (9.1%)
Other Intron (12.18%)
Downstream (<=300) (0.13%)
Distal Intergenic (13.06%)

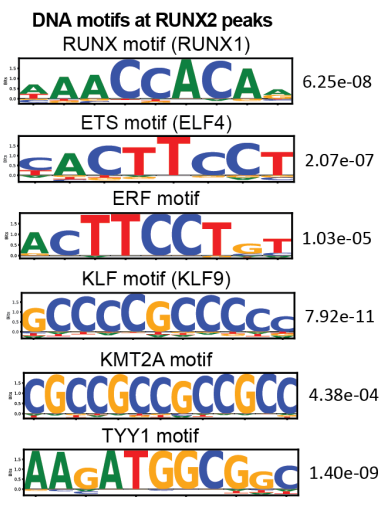
F
DNA motifs at RUNX2 peaks
RUNX motif (RUNX1)
6.25e-08
ETS motif (ELF4)
2.07e-07
ERF motif
1.03e-05
KLF motif (KLF9)
7.92e-11
KMT2A motif
4.38e-04
TYY1 motif
1.40e-09

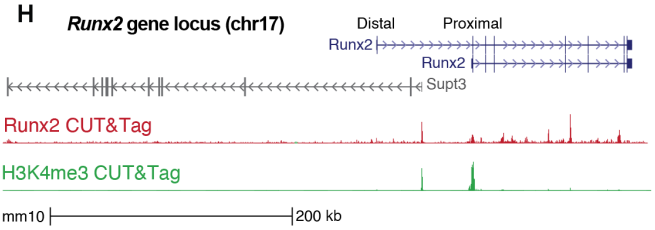
H
Runx2 gene locus (chr17)
Distal
Proximal
Runx2
Runx2
Supt3
Runx2 CUT&Tag
H3K4me3 CUT&Tag
mm10
200 kb

Figure 5

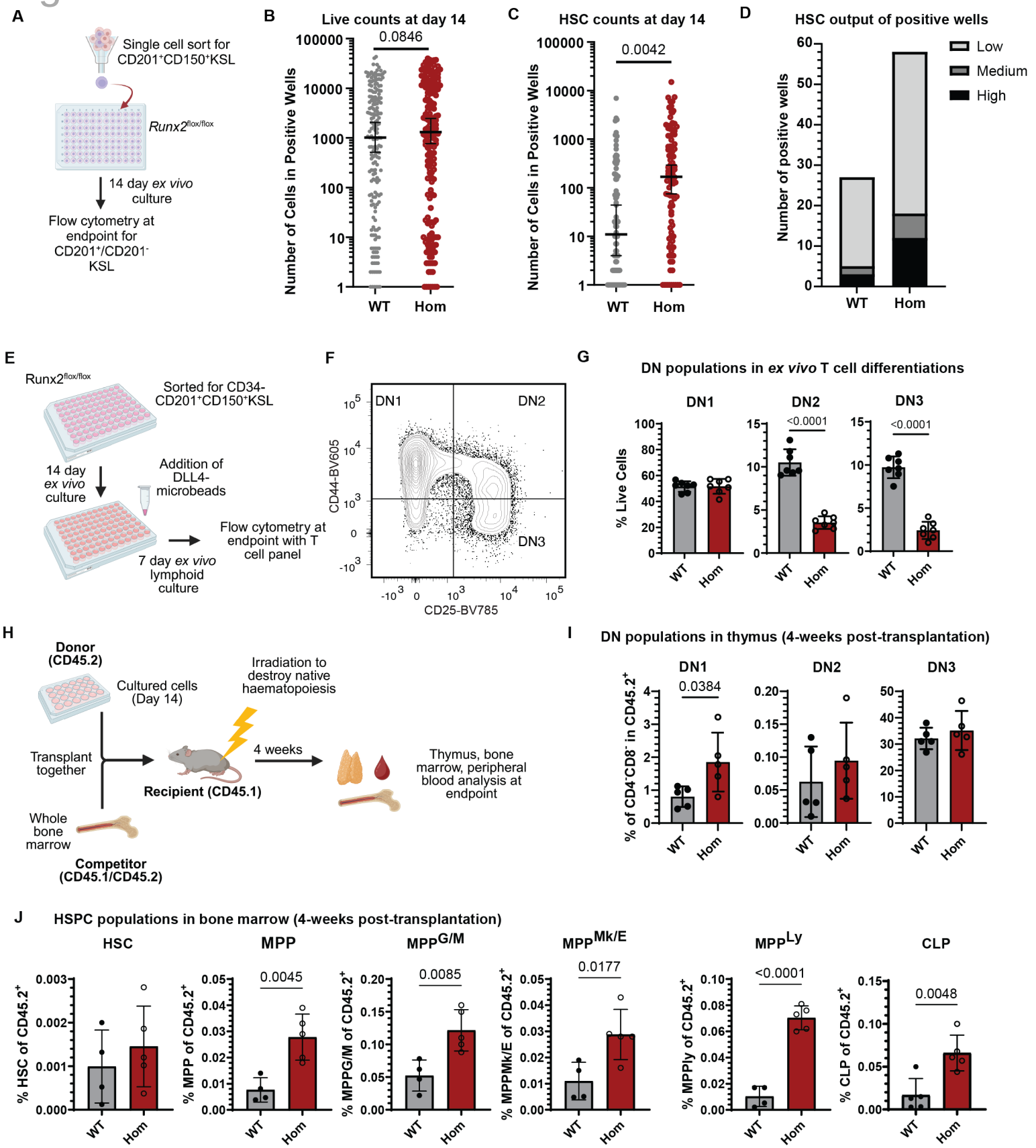
A
Single cell sort for CD201+CD150+KSL
Runx2flox/flox
14 day ex vivo culture
Flow cytometry at endpoint for CD201+/CD201- KSL
B
Live counts at day 14
0.0846
Number of Cells in Positive Wells
WT
Hom
C
HSC counts at day 14
0.0042
Number of Cells in Positive Wells
WT
Hom
D
HSC output of positive wells
Low
Medium
High
Number of positive wells
WT
Hom
E
Runx2flox/flox
Sorted for CD34- CD201+CD150+KSL
14 day ex vivo culture
Addition of DLL4-microbeads
7 day ex vivo lymphoid culture
Flow cytometry at endpoint with T cell panel
F
DN1
DN2
DN3
CD44-BV605
CD25-BV785
G
DN populations in ex vivo T cell differentiations
DN1
DN2
DN3
<0.0001
<0.0001
% Live Cells
WT
Hom
H
Donor (CD45.2)
Cultured cells (Day 14)
Irradiation to destroy native haematopoiesis
Transplant together
Recipient (CD45.1)
4 weeks
Thymus, bone marrow, peripheral blood analysis at endpoint
Whole bone marrow
Competitor (CD45.1/CD45.2)
I
DN populations in thymus (4-weeks post-transplantation)
DN1
DN2
DN3
0.0384
% of CD4-CD8- in CD45.2+
WT
Hom
J
HSPC populations in bone marrow (4-weeks post-transplantation)
HSC
MPP
MPPG/M
MPPMk/E
MPPLy
CLP
0.0045
0.0085
0.0177
<0.0001
0.0048
% HSC of CD45.2+
% MPP of CD45.2+
% MPPG/M of CD45.2+
% MPPMk/E of CD45.2+
% MPPly of CD45.2+
% CLP of CD45.2+
WT
Hom

Runx2 as a Regulator of Hematopoietic Stem Cell Expansion and T-Cell Commitment Identified by Genome-Wide Screening

Context of Research

- Hematopoietic stem cells (HSCs) are rare and hard to expand
- An *ex vivo* PVA-based system permits large-scale expansion
- Identifying negative regulators of expansion has biological and clinical relevance

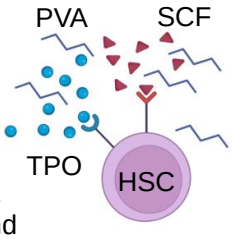

Methods

- Genome-wide CRISPR screen in PVA-based expansion system
- CRISPR-based *Runx2* knockout in HSCs
- Hematopoiesis-specific *Runx2* deletion

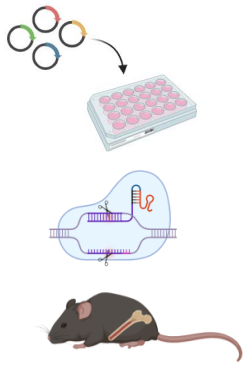

Main Findings

- Genome-wide CRISPR screen identified 92 putative negative regulators of *ex vivo* HSC expansion

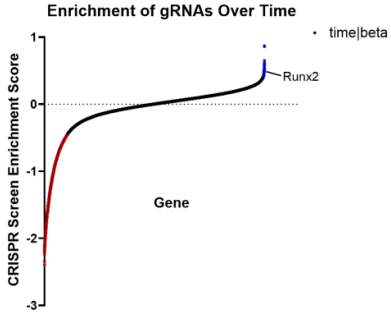

- *Runx2*-deficient HSCs have increased self-renewal *ex vivo* and increased engraftment *in vivo*

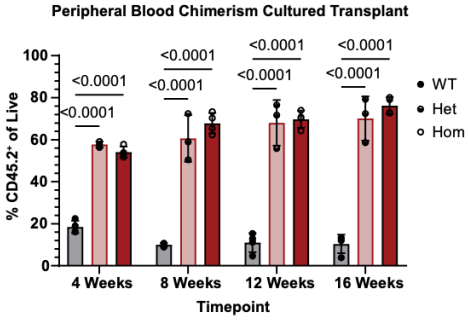

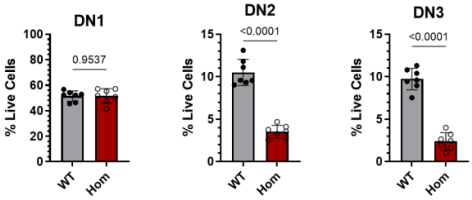

- *Runx2*-deficient HSCs are less able to produce T-cells

Conclusions: *Runx2*-deficient HSCs have a fitness advantage *ex vivo* and *in vivo* via increased self-renewal. *Runx2* is necessary for normal T-cell commitment

*Meaker et al. DOI: 10.xxxx/**blood**.2025xxxxxx*

blood Visual Abstract